One Hundred Inches in One Hundred Hours: Evolution of a Wasatch Mountain Winter Storm Cycle

W. JAMES STEENBURGH

NOAA/Cooperative Institute for Regional Prediction, and Department of Meteorology, University of Utah, Salt Lake City, Utah

(Manuscript received 29 August 2002, in final form 6 May 2003)

ABSTRACT

Synoptic, orographic, and lake-effect precipitation processes during a major winter storm cycle over the Wasatch Mountains of northern Utah are examined using radar imagery, high-density surface data, and precipitation observations from Alta Ski Area [2600–3200 m above mean sea level (MSL)] and nearby Salt Lake City International Airport (1288 m MSL). The storm cycle, which occurred from 22 to 27 November 2001, included two distinct storm systems that produced 108 in. (274 cm) of snow at Alta Ski Area, including 100 in. (254 cm) during a 100-h period. Each storm system featured an intrusion of low equivalent potential temperature (θ_e) air aloft, well in advance of a surface-based cold front. Prefrontal precipitation became increasingly convective as low-θ_e air aloft moved over northern Utah, while cold frontal passage was accompanied by a convective line and a stratiform precipitation region. Postfrontal destabilization led to orographic and lake-effect snowshowers that produced two-thirds of the observed snow water equivalent at Alta.

Storm stages were defined based on the passage of the above features and their accompanying changes in stability and precipitation processes. Contrasts between mountain and lowland precipitation varied dramatically from stage to stage and storm to storm, and frequently deviated from climatology, which features a nearly fourfold increase in precipitation between Salt Lake City and Alta. Based on the two storms, as well as other studies, a schematic diagram is presented that summarizes the evolution of Intermountain West snowstorms featuring an intrusion of low-θ_e air aloft ahead of a surface cold front. Implications for short-range quantitative precipitation forecasting and seasonal-to-annual hydrometeorological prediction are discussed.

1. Introduction

The Wasatch Mountains of northern Utah are one of interior North America's snowiest mountain ranges, averaging 520 in. (1320 cm) annually at Alta Ski Area in upper Little Cottonwood Canyon (Pope and Brough 1996; see Fig. 1 for locations). During major storm cycles, when a series of storms impact the Wasatch, accumulations can exceed 100 in. (254 cm). Dangerous avalanche conditions resulting from such heavy snowfall can result in the closure of state highways and the declaration of *interlodge* conditions, which legally restricts Alta residents and visitors to well-fortified buildings for avalanche protection. Such a storm cycle occurred from 22 to 27 November 2001 when two complex Intermountain West storm systems, enhanced during their late stages by the Great Salt Lake effect, produced 108 in. (274 cm) of snow at Alta. Because 100 in. (250 cm) of the total fell in a 100-h period, local news media and ski area marketing groups coined the phrase ''100 inches in 100 hours'' to describe the event. The storm cycle was the largest at Alta since 1991 and produced 15% of the snow water equivalent (SWE) that fell in local Salt Lake County watersheds during the winter 2001/02. The event also featured substantial lowland precipitation, with Salt Lake City International Airport (SLC) observing 1.27 in. (3.23 cm) of rainfall on 22 November, a record for a calendar day in that month.

Previous investigators have decomposed Intermountain West orographic snowstorms into stages based on stability, the passage of transient synoptic features, and/or precipitation processes. Marwitz (1980) and Cooper and Marwitz (1980) described the typical evolution of San Juan Mountains snowstorms through stable, neutral, unstable, and dissipating stages. During the *stable stage*, the low-level flow is fully or partially blocked and the ''effective height'' of a mountain barrier is reduced since orographic ascent on the windward slope of the barrier is limited to the region above the blocked flow. The storm tends to be heavily glaciated (i.e., consisting primarily of ice), precipitation particles grow primarily through vapor deposition, riming is light, and graupel formation is rare.

As the upstream flow destabilizes, San Juan storms reach their *neutral* and *unstable stages.* In the neutral stage, the blocked flow deteriorates and many orograph-

Corresponding author address: Dr. W. James Steenburgh, Dept. of Meteorology, 135 South 1460 East, Rm. 819, Salt Lake City, UT 84112-0110.
E-mail: jimsteen@met.utah.edu

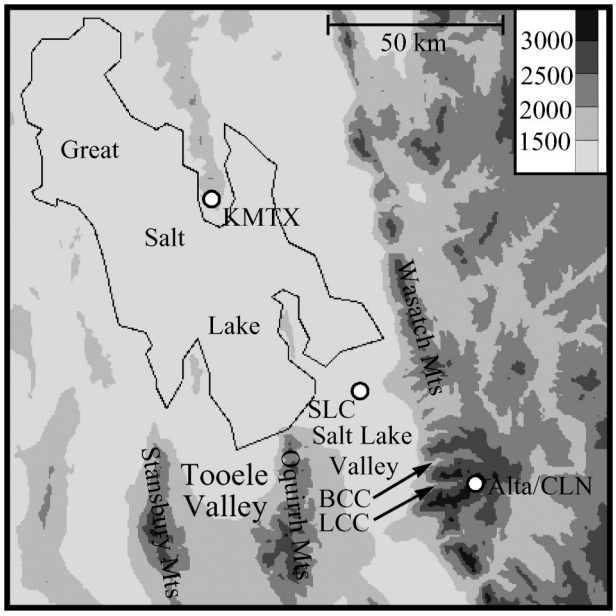

FIG. 1. Topographic and geographic features of northern UT. Abbreviations include SLC (Salt Lake City International Airport), BCC (Big Cottonwood Canyon), LCC (Little Cottonwood Canyon), KMTX (Promontory Point radar), and CLN (Collins observing site at Alta Ski Area). Elevation and distance based on scales at upper right.

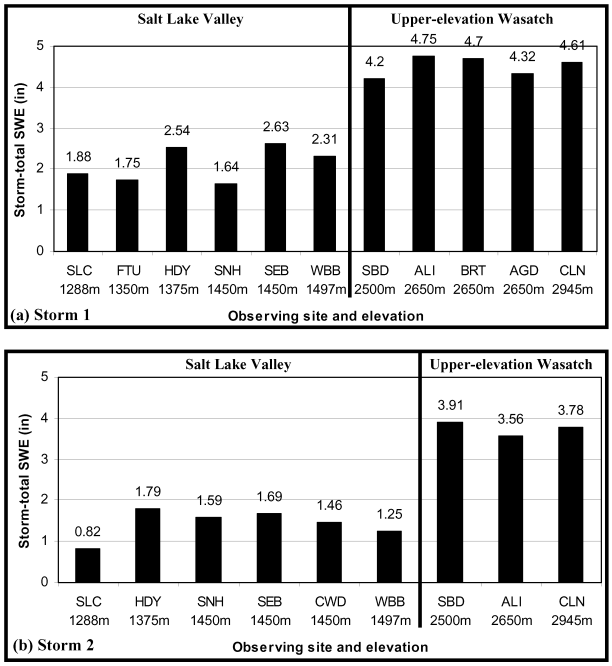

FIG. 2. Storm-total precipitation (SWE, in.) for (a) the first and (b) the second storm of the 100-in. storm cycle. Station abbreviations not defined in text are FTU, Fort Union; HDY, Holladay; SNH, Sandy; SEB, Salt Lake City East Bench; CWD, Cottonwood; WBB, University of Utah; SBD, Snowbird; ALI, Alta Lifts; BRT, Brighton; and AGD (Alta Guard). For the second storm, BRT did not report and AGD was removed for quality control reasons [reported precipitation was excessively high (L. Dunn 2002, personal communication)].

ic storms are at their deepest. The unstable stage is reached when the upstream flow becomes potentially unstable. A convergence zone and attendant convective line may form near the base of the windward side of the barrier. Otherwise, orographic lift releases the potential instability, resulting in convection and heavy orographic precipitation, which may be limited to over and very near the barrier. Because the vertical motion during the neutral and unstable stages is frequently deep and intense, riming and graupel formation may occur.

The approach and/or development of surface high pressure and upper-level ridging result in atmospheric stabilization and the onset of the *dissipating stage*. Atmospheric stabilization usually begins aloft, resulting in an increasingly shallow layer of potential instability and more widely scattered orographic snowshowers. Eventually, the available instability becomes too weak and shallow to develop precipitating clouds, leaving only shallow cumulus over the mountain barrier.

Hobbs (1975) describes a similar storm evolution for winter storms over the Cascade Mountains, but denotes the storm stages as prefrontal, transitional, and unstable, which roughly correspond to the stable, neutral, and unstable stages identified by Marwitz (1980). Compared with snowstorms over Intermountain West ranges, Cascade and Sierra Nevada snowstorms feature more riming and lower ice particle concentrations due to their warmer temperatures and maritime cloud condensation nuclei (CCN) concentrations (e.g., Hobbs 1975; Marwitz 1980, 1986).

The conceptual model of Marwitz (1980) and Marwitz and Cooper (1980) was based on events that featured the passage of a baroclinic zone that was confined to the middle and upper troposphere. In contrast, Long et al. (1990) and Sassen et al. (1990) examined a winter storm over the Tushar Mountains of south-central Utah that featured the passage of what they termed an upper-level cold surge/humidity front, which was followed several hours later by a surface-based cold front. This series of upper-level and surface-based features resulted in a more complex evolution of stability and precipitation processes, including a period where mesoscale precipitation bands associated with the surface-based cold front produced heavy snowfall (Sassen et al. 1990).

A unique aspect of some Wasatch Mountain snowstorms is the influence of the Great Salt Lake. Lake-effect snow typically occurs in unstable, postfrontal, northwesterly flow, with heat and moisture fluxes over the lake surface acting to either create or enhance potential instability. In some cases, intense *midlake snowbands* develop along the lake axis and extend downstream over the Salt Lake valley and Big and Little Cottonwood Canyons (Steenburgh et al. 2000; see Fig. 1 for locations). Such bands usually develop during the overnight and early morning hours due to overlake land-breeze convergence (Steenburgh and Onton 2001). Oro-

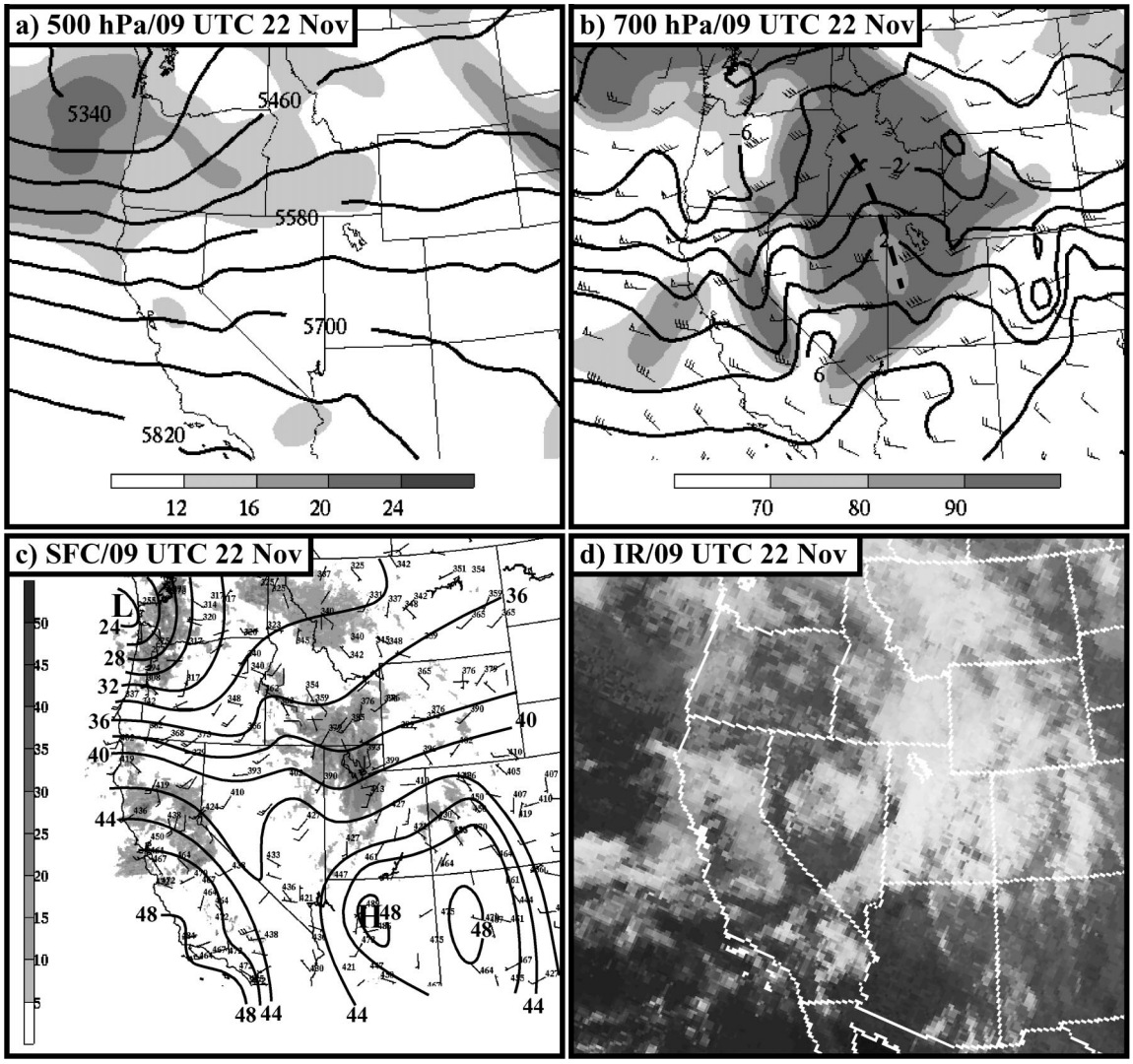

FIG. 3. Manual surface, RUC2 upper-level, and satellite analyses at 0900 UTC 22 Nov 2001. (a) The 500-hPa geopotential height (every 60 m) and absolute vorticity ($\times 10^{-5}$ s^{-1}, shaded following scale at bottom). (b) The 700-hPa temperature (every 2°C), wind (full and half barbs denote 5 and 2.5 m s^{-1}, respectively), and relative humidity (%, shaded following scale at bottom). Thermal ridge axis denoted by heavy dashed line. (c) Manual 1500-m pressure analysis (every 2 hPa) and composite radar reflectivity (dBZ, shaded following scale at left). Station observations include wind barbs [as in (b)] and 1500-m pressure (tenths of hPa with leading 8 omitted). (d) Infrared satellite image (using linear enhancement curve).

graphic precipitation enhancement can occur within midlake bands when they intersect downstream mountain ranges (Onton and Steenburgh 2001).

This paper uses radar imagery, high-density surface data collected by the Mesowest cooperative networks (Horel et al. 2002), and precipitation observations from SLC and Alta Ski Area (see Fig. 1 for locations) to describe the evolution of the 22–27 November 2001 storm cycle. After a review of the data and methods used in the next section, it will be shown in section 3 that the storm cycle was produced by two distinct storm systems, each featuring an intrusion of low equivalent potential temperature (θ_e) air aloft that was followed several hours later by a surface-based cold frontal passage. Precipitation rates and characteristics varied widely with the passage of these features and their accompanying changes in atmospheric stability, with orographic and lake-effect processes during unstable post-cold-frontal stages producing the majority (63%) of the SWE that was observed at Alta Ski Area. In section 4, the evolution of the two storm systems is compared to that described by earlier work, with findings summarized by a schematic diagram. Possible implications for short-range quantitative precipitation forecasting and seasonal-to-annual hydrometeorological prediction are also discussed.

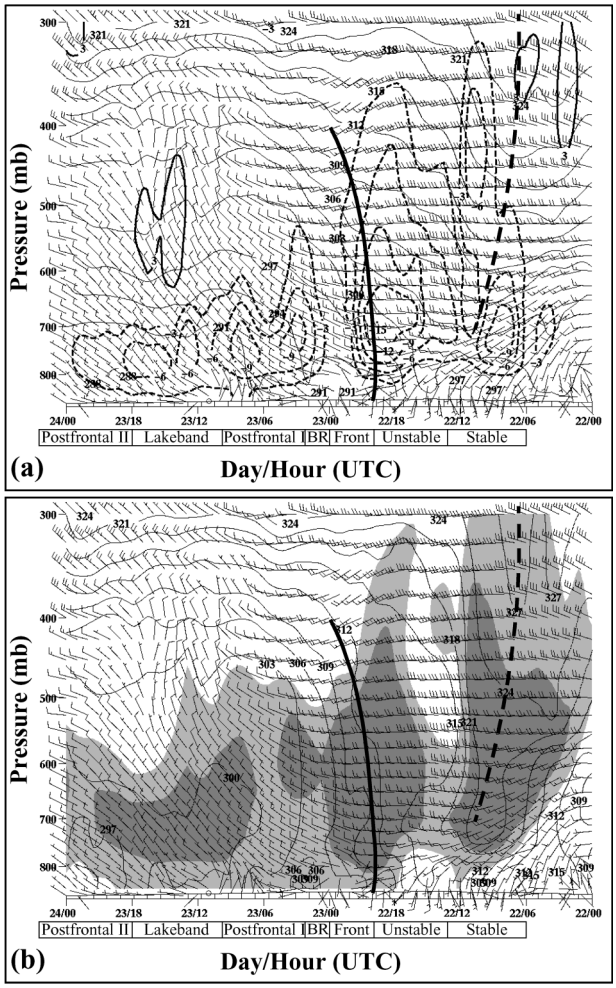

FIG. 4. RUC2 time–height section analyses at SLC from the first storm (0000 UTC 22 Nov–0000 UTC 24 Nov 2001). (a) Potential temperature (thin contours every 3 K), vertical velocity (ω, $\times 10^{-1}$ Pa s^{-1}, thick contours every 3×10^{-1} Pa s^{-1} with negative contours dashed), and wind barbs (full and half barbs denote 2.5 and 5 m s^{-1}, respectively). (b) The θ_e (every 3 K), relative humidity (light and dark shading denote >70% and >90%, respectively), and wind barbs [as in (a)]. Heavy dashed and solid lines denote warm tongue axis aloft and surface-based cold front, respectively.

2. Data and methods

Surface observations used for the manual analyses presented in this paper were provided by the Mesowest cooperative networks, which, during the study period, collected observations from more than 70 networks and 2800 stations in the western United States (Horel et al. 2002). Surface analysis methods followed those described by Steenburgh and Blazek (2001), including the use of 1500-m pressure (derived from altimeter setting, station elevation, and the *U.S. Standard Atmosphere*) instead of sea level pressure. Gridded analyses produced by the Rapid Update Cycle version 2 (RUC2; Benjamin et al. 1998), which were available hourly at 60-km horizontal and 25-hPa vertical grid spacings, were used for upper-air analyses and time–height sections that illustrate the large-scale conditions over northern Utah and the western United States. Vertical motion in time–height sections is based on the initial vertical motion in the RUC2 analysis. The RUC2 analyses were supplemented by observed soundings from SLC (available every 12 h) and manual streamline analyses at times when important mesoscale circulations were evident.

Precipitation structures associated with distinct storm stages were identified using lowest elevation (0.5°) base reflectivity imagery from the KMTX National Weather Service (NWS) Weather Surveillance Radar-1988 Doppler (WSR-88D; Crum and Alberty 1993). KMTX is located atop Promontory Point at an elevation of 2004 m above sea level (MSL), approximately 724 m above the Great Salt Lake and 716 m above SLC (Fig. 1). Analysis complications arise from the radar's high-elevation location, topographic beam blockage, and brightband contamination (e.g., Dunn and Vasiloff 2001) and are discussed as necessary in the manuscript. Lowest elevation (0.5°) base reflectivity mosaics for the western United States are also subject to the above analysis complications. In particular, there are large regions with no radar coverage including portions of eastern Oregon, central Idaho, central Utah, and central Nevada.

Hourly SWE observations from SLC (1288 m MSL) and the Collins observing site at Alta Ski Area (CLN, 2946 m MSL) are used to compare and contrast lowland and mountain precipitation rates (see Fig. 1 for locations). SLC is the lowest observing site in the Salt Lake valley and is located just south of the Great Salt Lake. Precipitation observations were collected by an Automated Surface Observing System (ASOS) heated tipping bucket. Since the ASOS heated tipping bucket exhibits problems measuring frozen precipitation, 24-h precipitation totals were compared to daily local climate data provided to the National Climatic Data Center (NCDC) by the NWS SLC Forecast Office. The latter uses manual snow-core observations instead of ASOS observations when deemed necessary. Only the 24-h period ending at 0700 UTC 26 November exhibited a discrepancy, with ASOS reporting 0.78 in SWE and the SLC Forecast Office reporting 0.90 in SWE. Hourly ASOS observations may underestimate (by ~15%) actual precipitation during this period.

CLN is located in a basin near the upper terminus of Little Cottonwood Canyon and is the highest precipitation observing site in the Wasatch Mountains. The site was installed and maintained by the Alta Ski Area Snow Safety Staff and features an ETI Instrument Systems Inc. Noah II Total Precipitation Gauge. Antifreeze within the gauge melts incoming snow with SWE measured by a pressure sensor. A device that circulates the water–antifreeze mixture helps prevent slush development and snow buildup on the gauge walls. The instrument is ringed by a standard wind shield, located in a well-sheltered open area, and checked regularly by members of the Alta Ski Patrol. Snowfall observations are based

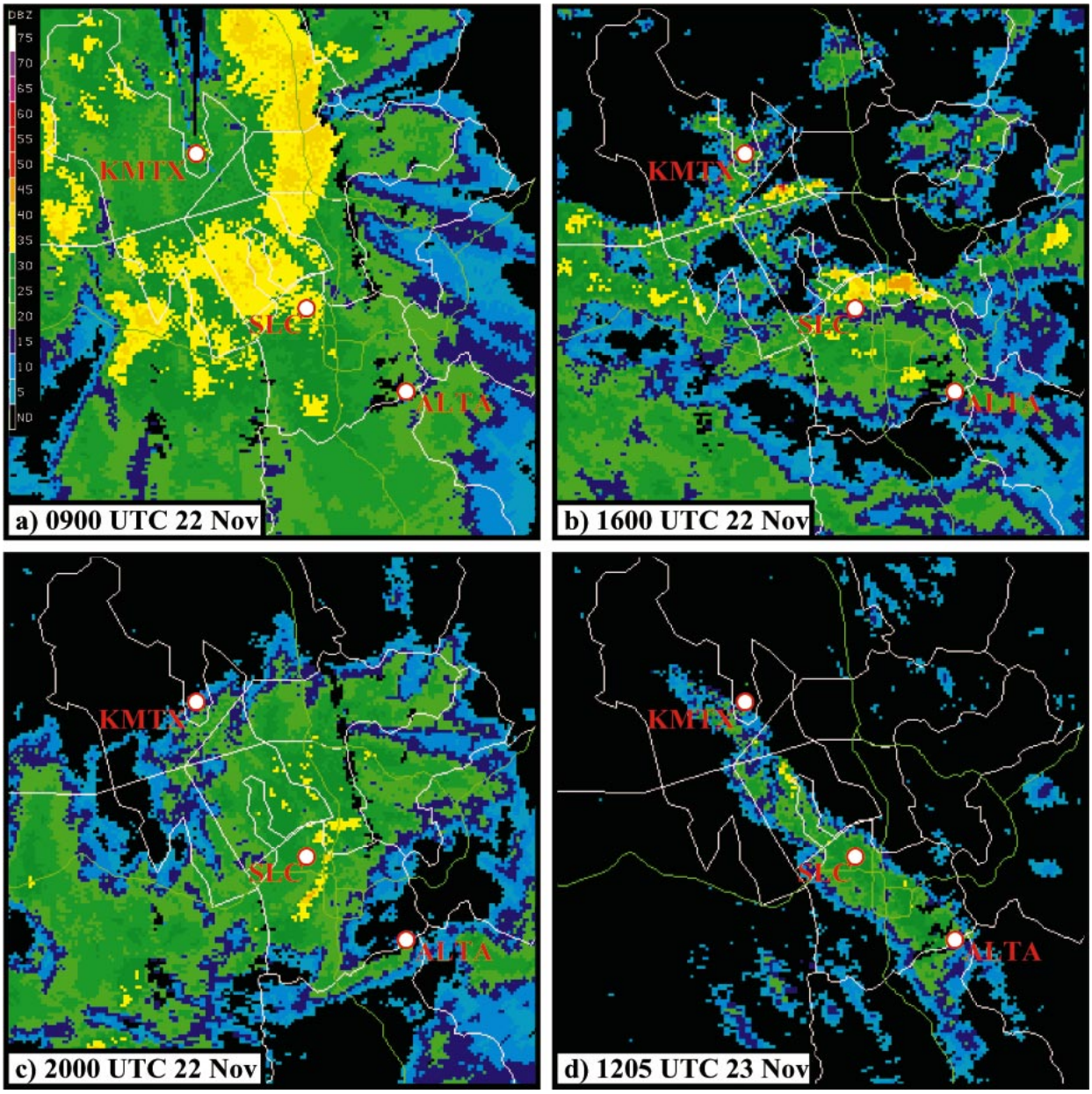

FIG. 5. KMTX lowest-elevation angle (0.5°) base reflectivity analyses at (a) 0900 UTC 22 Nov, (b) 1600 UTC 22 Nov, (c) 2000 UTC 22 Nov, and (d) 1205 UTC 23 Nov 2001. Scale at upper left of (a).

on manual observations collected by the Alta Snow Safety Staff every 12 h (~0000 and 1200 UTC) at an established measurement site at the base of the ski area (2610 m MSL). This site is located 2 km north of and 336 m lower than CLN.

Since precipitation contrasts between SLC and CLN may arise from factors other than orographic processes (e.g., the position and orientation of lake-effect snowbands), efforts were undertaken to determine the representativeness of these sites. Unfortunately, SLC and CLN were the only stations in the Salt Lake valley and adjoining upper-elevation Wasatch Mountains that provided reliable hourly precipitation observations during the study period.[1] Therefore, quantitative assessment of

[1] Mesowest provided hourly precipitation observations from seven additional sites in the region. Three were snow telemetry (SNOTEL) sites that were designed for seasonal applications and were found unsuitable for this high-frequency application. The remaining four were automated sites that either substantially underreported precipitation (based on comparison to storm-total manual observations) or showed evidence of substantial snow buildup on gauge sidewalls or rims that prevented proper apportionment of precipitation on a stage-by-stage basis. Estimated (based on manual inspection and adjustment of the automated observations) storm-total precipitation from two

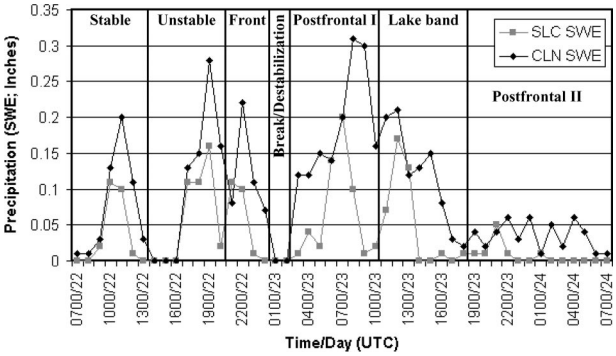

FIG. 6. Hourly accumulated precipitation (SWE, in.) at SLC and CLN during the first storm. Major stages annotated.

representativeness for individual storm stages was not possible. Analysis of available spotter and cooperative storm-total precipitation for each storm showed, however, that SLC was generally representative of the precipitation over the Salt Lake valley (Fig. 2). It was one of the drier locations, but this is consistent with the fact that the other valley sites are located at higher elevations, are closer to the steep windward slope of the Wasatch Mountains (not shown), and typically receive more precipitation climatologically [annually averaged precipitation (SWE) at SLC is 16.2 in., compared with up to 25 in. at the other Salt Lake valley sites]. Note that the precipitation minimum at SLC during the second storm is somewhat exaggerated due to the estimated 15% underreporting by the ASOS gauge, as described earlier. At CLN, storm-total precipitation from both storms was comparable to other upper-elevation sites. Thus, on a storm by storm basis, observations from SLC and CLN appear to reflect their respective lowland and mountain locations, with their contrasts a reasonable estimate of the overall orographic precipitation contrast.

During individual storm stages, the impact of variability in the strength, position, and evolution of precipitation features such as lake-effect snowbands on precipitation at CLN and SLC was examined qualitatively using radar imagery and the less reliable gauge data from nearby sites. Times where such variability appeared significant are noted where appropriate in section 3.

3. Storm cycle evolution

a. The initial strike

The first storm occurred from 0600 UTC 22 November to 0700 UTC 24 November and produced 50 in. (127 cm) of snow at the base of Alta Ski Area. At 0900 UTC 22 November, during the initial stable stage of the storm, a 500-hPa shortwave trough and absolute vorticity maximum were located off the Pacific Northwest coast (Fig. 3a). Attendant with these features was a mature surface cyclone that was centered near the southwest Washington coast (Fig. 3c). The surface occluded front associated with this system made landfall around 0000 UTC and weakened as it moved inland. Due to a lack of surface definition, this occlusion was not analyzed in the 0900 UTC surface analysis (Fig. 3c). Evidence of the occluded front was, however, found at 700 hPa where a warm tongue extended northward along the Utah–Nevada border into central Idaho (Fig. 3b), and in the RUC2-based time–height section from SLC that illustrated that the warm tongue possessed a forward-sloping structure resembling a warm occlusion (Fig. 4a). Extensive cirrostratus, representing the remnants of the cyclone's comma-shaped cloud deck, was found downstream of the warm tongue and extended southwestward across southern Nevada (Fig. 3d).

Vertical motion (ω) maxima accompanied the low-level (800–600 hPa) zone of warm advection ahead of

sites impacted by the latter problem, SNH and WBB, is presented in Fig. 2.

TABLE 1. Precipitation characteristics of the major stages of the first storm.

Stage and time period	CLN SWE (in.)	CLN mean SWE rate (in. h^{-1})	Contribution to CLN storm total SWE (%)	SLC SWE (in.)	SLC mean SWE rate (in. h^{-1})	Contribution to SLC storm total SWE (%)	Orographic enhancement (CLN/SLC) (%)
Stable, 0600–1300 UTC 22 Nov	0.52	0.074	11.3	0.24	0.034	12.8	217
Unstable prefrontal, 1300–2000 UTC 22 Nov	0.72	0.180	15.6	0.40	0.100	21.3	180
Frontal passage, 2000 UTC 22 Nov–0000 UTC 23 Nov	0.48	0.120	10.4	0.22	0.055	11.7	218
Break, 0000–0200 UTC 23 Nov	0	0	0	0	0	0	—
Postfrontal I, 0200–1000 UTC 23 Nov	1.50	0.188	32.5	0.54	0.068	28.7	278
Midlake band, 1000–1800 UTC 23 Nov	0.94	0.118	20.4	0.39	0.049	20.7	241
Postfrontal II, 1800 UTC 23 Nov–0700 UTC 24 Nov	0.45	0.035	9.8	0.09	0.007	4.8	500
Total, 0600 UTC 22 Nov–0700 UTC 24 Nov	4.61	0.094	100	1.88	0.038	100	245

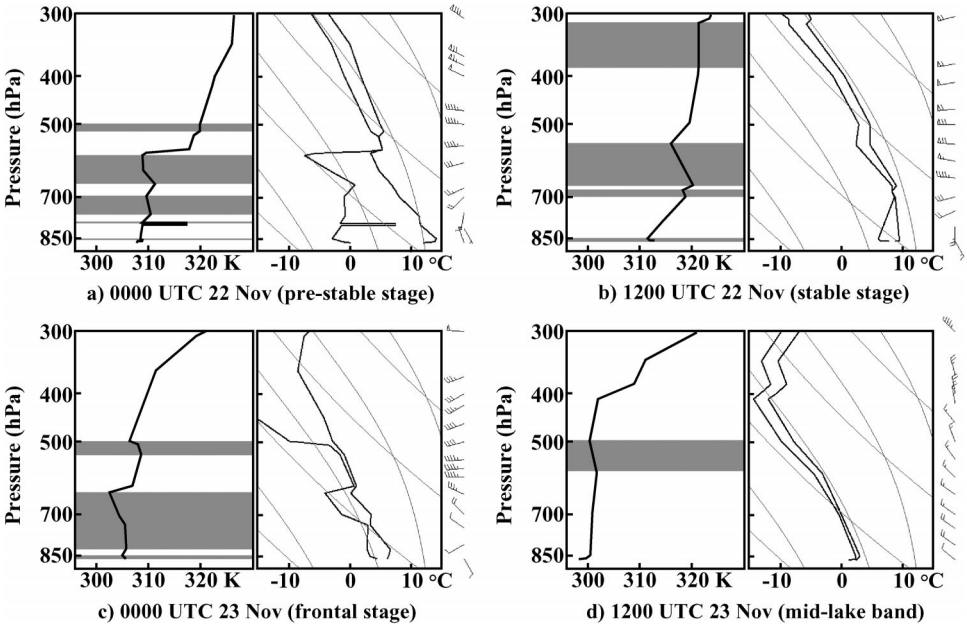

FIG. 7. Observed SLC θ_e profile and skew T–log$p$ diagram [temperature, dewpoint, and wind barbs (full and half barbs denote 5 and 2.5 m s^{-1}, respectively)] at (a) 0000 UTC 22 Nov, (b) 1200 UTC 22 Nov, (c) 0000 UTC 23 Nov, and (d) 1200 UTC 23 Nov 2001. Layers with constant or decreasing θ_e with height denoted with gray shading. Dry and moist adiabats identified with thin lines.

the warm tongue, and the upper-level (500–300 hPa) zone of cold advection that trailed the warm tongue as they passed over SLC (Fig. 4a). The former was consistent with large-scale ascent associated with the temperature advection term of the quasigeostrophic omega equation (Holton 1992, 166–170). The latter, however, was not consistent with quasigeostrophic dynamics because it was found in a region with cold advection and weak differential vorticity advection where one would infer subsidence (not explicitly shown). Instead, it is possible that smaller-scale processes, such as those described by Stoelinga et al. (2000) for a cold front aloft over the central United States, were responsible for the ascent.

Widespread valley rain and mountain snow (the latter above ~2500 m) developed as lower-tropospheric warm advection and large-scale ascent ahead of the warm tongue moved over northern Utah (Fig. 5a). Although Fig. 5a shows that radar reflectivities were highest mainly over low-elevation regions, the observed precipitation at CLN during this stage was more than double that observed at SLC (Table 1, Fig. 6). This poor correlation between lowest-elevation radar reflectivity and observed precipitation was the result of at least two factors. First, the higher reflectivities (>35 dBZ) that encircle the KMTX radar site were the result of brightband contamination since the melting layer was located near 2500 m. Second, because of the altitude of the radar site and slope of the beam relative to the earth's surface (see section 2), the observed reflectivities were produced by hydrometeors that were well above valley level. Considerable hydrometeor sublimation and evaporation likely occurred over the Salt Lake valley since 10°–15°C dewpoint depressions were evident below 600 hPa prior to precipitation onset (Fig. 7a). This hydrometeor sublimation and evaporation was one contributor to the observed precipitation contrast between SLC and CLN during this stage. Another contributor may have been orographic precipitation enhancement within upslope flow that existed at upper elevations. Mesowest observations (not shown) and the 1200 UTC sounding (Fig. 7b) revealed that, although valley flows were weak or terrain parallel, at crest level (700 hPa), cross-barrier westerly to southwesterly flow was evident. Thus, orographic upslope was likely at mid- or upper elevations, as observed during other Wasatch Mountain winter storms (e.g., Cox 2002).

Following passage of the 700-hPa warm tongue axis, upward vertical velocity weakened in the lower troposphere (Fig. 4a) and no measurable precipitation was observed at SLC and CLN from 1300 to 1600 UTC 22 November (Fig. 6). During this period, a layer of potential instability, which extended from 675 to 550 hPa at 1200 UTC 22 November (Fig. 7b), deepened as low-θ_e air moved in aloft (above 700 hPa) and warm advection and solar insolation increased the low-level θ_e (Fig. 4b). By 1600 UTC 22 November, precipitation began to fall at SLC and CLN (Fig. 6). The precipitation was scattered and convective in nature, with a few strong convective cores reaching more than 35 dBZ (e.g., Fig. 5b). Convective initiation was not confined, however, to over the mountains and the SWE contrast between

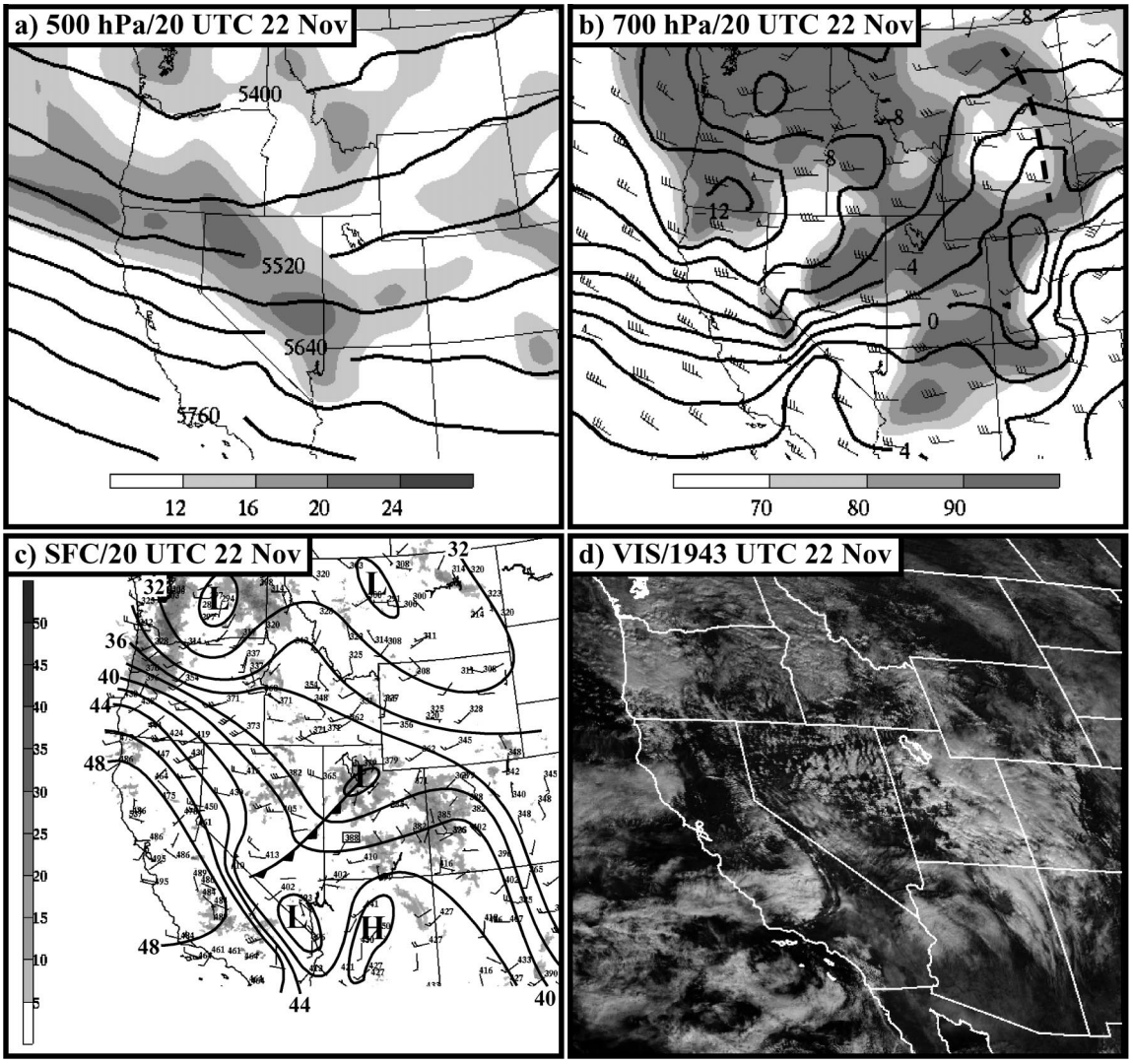

FIG. 8. Same as in Fig. 3 except for 2000 UTC 22 Nov 2001, image in (d) is visible, and Milford, UT (MLF), is identified in (c) with a box around the 1500-m pressure observation.

SLC and CLN was smaller during this period than any other stage of the storm (Fig. 6, Table 1). Although the destabilization was confined to the 675–550-hPa layer, strong vertical motion in advance of an approaching 500-hPa absolute vorticity maximum provided the necessary lift for convective initiation to occur over both the mountains and lowlands (Figs. 4a, 8a). We refer to this period, which extends from 1300 to 2000 UTC 22 November, as the unstable stage due to the dominant role played by convective precipitation processes.

By 2000 UTC 22 November, the synoptic pattern over the western United States was quite complex. At the surface, the primary low center had moved into central Washington and a lee cyclone was beginning to form over Montana (Fig. 8c). A secondary low center was located over northern Utah beneath an area of 500-hPa cyclonic absolute vorticity advection (cf. Figs. 8a,c). A cold front, which appeared to develop over central and eastern Nevada, extended from the secondary low center southwestward to the Sierra Nevada. Baroclinity, cold advection, and the θ_e gradient accompanying the cold front were strongest at midlevels (700–400 hPa; Figs. 4a,b). At the surface, the frontal passage was more complex and diffuse. At SLC, where passage of a convective line resulted in a pressure rise and cooling at 1600 UTC, a pressure check and 2.5°C temperature fall were observed with frontal passage (Fig. 9a, 2000 UTC). Postfrontal winds were initially northerly, but terrain-channeled southerly flow resumed for 3 h as the large-scale poleward-directed pressure gradient acceleration became reestablished following frontal passage. Northerly winds redeveloped around 0200 UTC 23 November. Farther to the south, where prefrontal convection was less widespread and intense, Milford (see Fig. 8c for

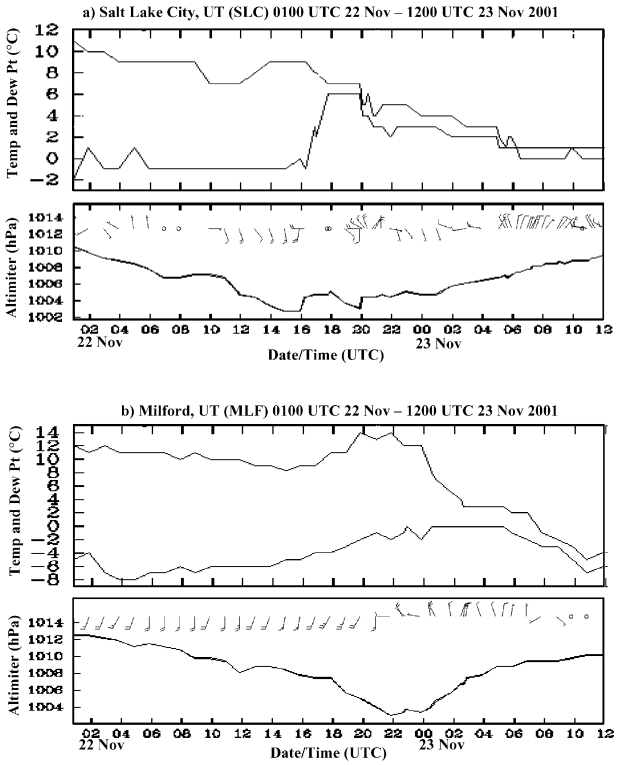

FIG. 9. Time series of (upper) temperature and dewpoint and (lower), altimeter setting and wind barbs (full and half barbs denote 2.5 and 5 m s^{-1}, respectively) at (a) SLC and (b) MLF from 0100 UTC 22 Nov to 1200 UTC 23 Nov 2001.

location) observed pressure minima at 2200 UTC 22 November and 0000 UTC 23 November (Fig. 9b). The former marked the initial veering of surface winds, whereas a second wind shift and rapid cooling followed the latter.

Although significant clouds and precipitation were not organized along the front in Nevada (e.g., Fig. 8d), cold-frontal passage over northern Utah was accompanied by a convective snowband with radar reflectivities exceeding 35 dBZ (Fig. 5c). Behind this feature, lower reflectivities (and more uniform, light precipitation) extended upstream for about 50 km. Because frontal dynamics appeared critical to the generation of precipitation during this period, we refer to it as the frontal stage. Nevertheless, orographic precipitation enhancement within the frontal precipitation zone resulted in twice as much SWE at CLN as at SLC (Table 1 and Fig. 6).

Figure 7c illustrates the upper-level conditions over SLC roughly 3 h following frontal passage when frontal precipitation was ending. Backing winds between 750 and 400 hPa implied a deep layer of middle-tropospheric cold advection. Veering winds near the surface were the result of low-level terrain channeling as the large-scale poleward-directed pressure gradient acceleration became reestablished following frontal passage. Potential instability was present from 775 to 650 hPa, although precipitation ended for a 2-h period beginning at 0000 UTC 23 November (Fig. 6 and Table 1) as low-level relative humidity decreased and upward vertical motion weakened (Fig. 4).

Precipitation redeveloped after 0200 UTC 23 November as postfrontal northwesterly flow intensified, potential instability deepened (Fig. 4b), and orographic and lake-effect processes contributed to the development of snowshowers that were heaviest and most frequent over the Wasatch Mountains and to the lee of the Great Salt Lake (not shown). RUC2-analyzed upward vertical motion also strengthened during this period (Fig. 4a), although this may be a reflection of northwesterly flow ascending the highly smoothed RUC2 terrain gradient that extends well upstream of the actual Wasatch slope. Nevertheless, strengthening orographic ascent near and over the Wasatch Mountains is implied by increasing northwesterly flow. This period, which we refer to as postfrontal stage I, extended from 0300 to 1000 UTC 23 November and produced 33% of the SWE observed at CLN during this first storm (Table 1). A significant fraction of this precipitation was produced by lake-effect snowbands.

Beginning at 1000 UTC 23 November, precipitation was produced almost exclusively by a midlake snowband that, at 1200 UTC 23 November, extended along the major lake axis, over the Salt Lake valley, and into the Big and Little Cottonwood Canyons (Fig. 5d). This band developed when Utah was well north of the polar jet and under large-scale northwesterly flow at both 500 and 700 hPa (Figs. 7d, 10a,b). Observed lake temperatures were near 7.5°C (not shown) and 700-hPa temperatures were around −9°C (Fig. 10b), resulting in a lake −700-hPa temperature difference of 16.5°C, just meeting the threshold considered necessary for lake-effect precipitation over the Great Salt Lake (Steenburgh et al. 2000). The SLC upper-air sounding, taken in or very near the snowband, showed near-moist-neutral conditions from just above the surface layer to almost 400 hPa (Fig. 7d). The necessary lift to initiate convection was implied by the apparent midlake convergence of strong west-northwesterly flow over the western half of the lake with light offshore flow from the eastern shoreline (Fig. 10c).

Although this midlake band was an impressive feature, hourly averaged precipitation rates at CLN and SLC were actually weaker than observed prior to its development (cf. postfrontal I and lakeband periods; Fig. 6). This was because SLC and CLN did not remain under the snowband axis for prolonged periods of time. Nevertheless, almost all of the SWE observed at CLN during this period, which amounts to 22% of the storm total, can be attributed to the midlake band and embedded orographic enhancement. Since a significant fraction of the precipitation during postfrontal stage I was produced by lake-effect or lake-enhanced precipitation, it appeared that at least one-third of the precip-

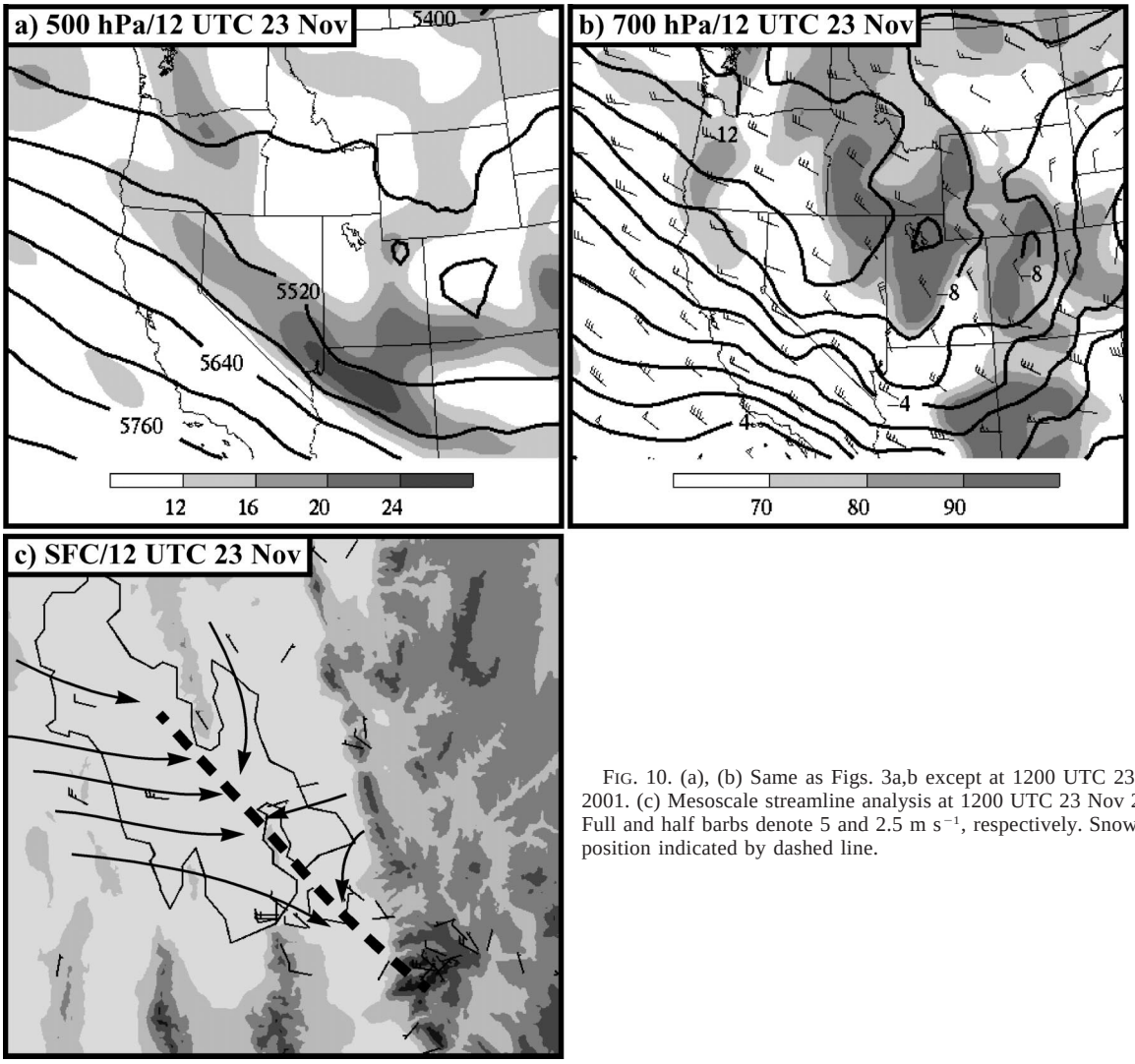

FIG. 10. (a), (b) Same as Figs. 3a,b except at 1200 UTC 23 Nov 2001. (c) Mesoscale streamline analysis at 1200 UTC 23 Nov 2001. Full and half barbs denote 5 and 2.5 m s^{-1}, respectively. Snowband position indicated by dashed line.

itation during this first storm was initiated by processes associated with the Great Salt Lake.

Postfrontal stage II began at 1800 UTC 23 November when the midlake band weakened rapidly, potential instability appeared to be released primarily by orographic lift, and precipitation became increasingly confined to the mountains. The importance of orographic forcing is further highlighted by the fact that this period featured the largest contrast between mountain and valley precipitation, with CLN receiving more than 5 times as much SWE as SLC (Table 1).

In total, precipitation in the unstable northwesterly flow following passage of the frontal precipitation zone produced 63% of the total precipitation observed at CLN. Just over 20% of the storm total was produced exclusively by the midlake snowband and its interaction with the Wasatch Mountains, with an additional 33% produced by both lake and orographic processes during postfrontal stage I. Thus, orographically enhanced lake-effect snowbands were responsible for at least one-third of the snowfall produced at CLN during this storm.

b. The grand finale

After 12 h with little or no accumulation at mountain locations, a second storm system moved into the region, producing 58 in. (147 cm) of snow at the base of Alta Ski Area from 1900 UTC 24 November to 0300 UTC 27 November. The surface cyclone associated with this storm developed off the California coast and deepened as it moved inland and traversed the high topography of northern California and Nevada. By 2100 UTC 24 November, just after the onset of precipitation at CLN, the surface cyclone was centered near the California–Oregon border with a 500-hPa trough located over the U.S. west coast (Figs. 11a,c). The low-level remnants of the Pacific occluded front were merging with a lee trough that extended from the low center through west-

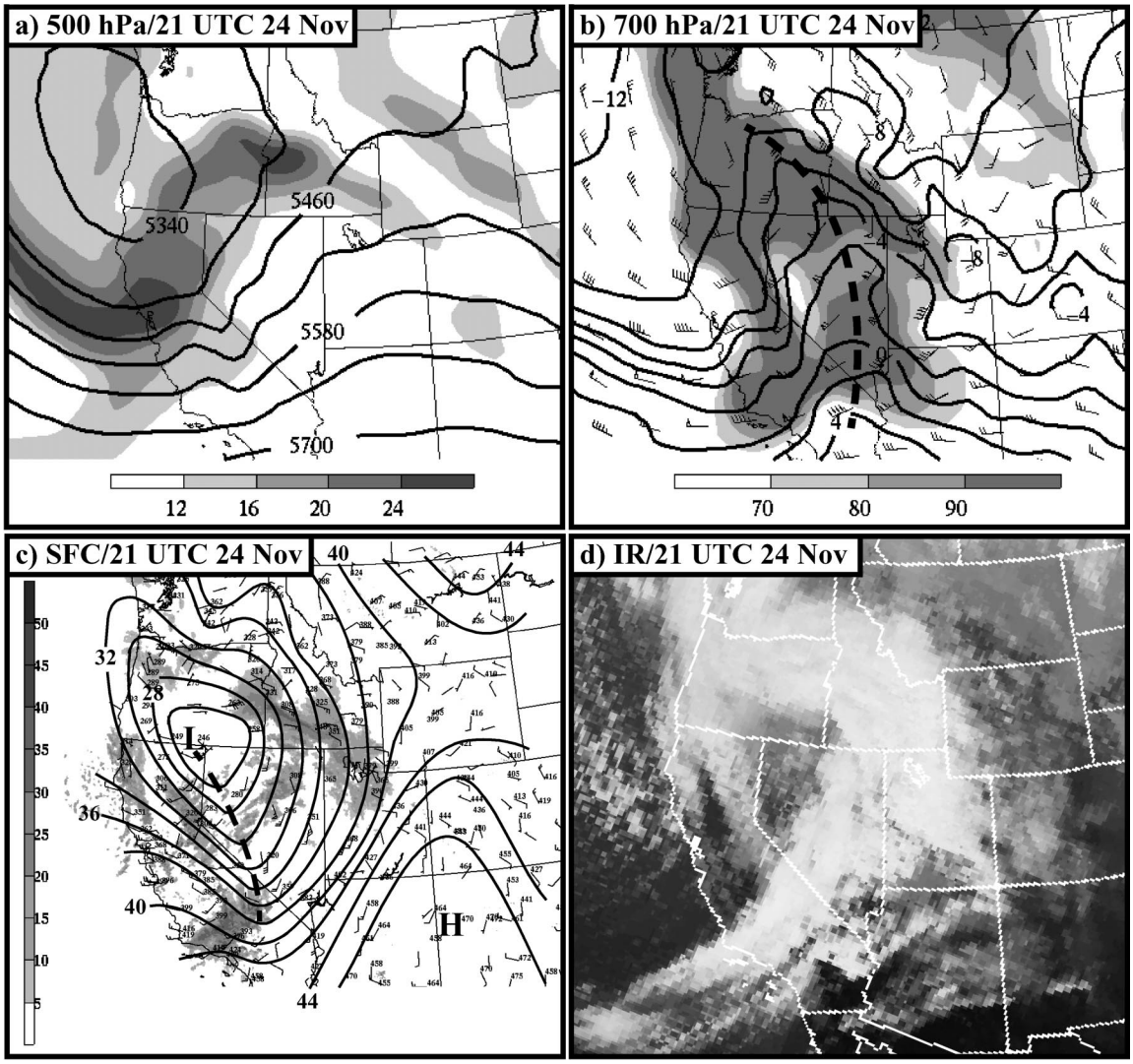

FIG. 11. Same as in Fig. 3 except at 2100 UTC 24 Nov 2001.

ern Nevada (Fig. 11c). The comma-shaped cirrostratus deck accompanying the system was relatively well developed (Fig. 11d) and characteristic of the later stages of cyclogenesis (e.g., Wallace and Hobbs 1977, 261–262). Over northern Nevada, the leading edge of the dry slot and back edge of the cirrostratus deck were already located ahead of the surface trough. Also ahead of the surface trough was a warm tongue that was evident at 700 hPa (Fig. 11b) and throughout the middle and upper troposphere, but did not appear to extend to the ground (Fig. 12a). Trailing the warm tongue was the leading edge of low-θ_e air aloft (Figs. 12a,b).

Large-scale ascent associated with lower- to middle-tropospheric warm advection ahead of the warm tongue (Figs. 11b, 12a) produced virga or light precipitation across much of northern Utah. Radar returns during this stable stage were weak (25 dBZ or less), horizontally uniform, and indicative of stratiform precipitation (Fig. 13a). During this stage, which extended to 0500 UTC 25 November, a significant contrast between lowland and mountain precipitation was observed. CLN recorded 0.54 in. (1.37 cm) SWE, whereas SLC recorded no measurable precipitation (Fig. 14, Table 2). Subcloud hydrometeor sublimation and evaporation in the subsaturated air mass that was resident over the Salt Lake valley was one likely contributor to this contrast, similar to the first storm. The SLC sounding prior to precipitation onset (1200 UTC 24 November) showed dewpoint depressions of ~8°C below 700 hPa (Fig. 15a). About 3 h after precipitation onset (0000 UTC 25 November), dewpoint depressions below 700 hPa were smaller, but remained around ~3°C (Fig. 15b).

Passage of the leading edge of low-θ_e air aloft (above ~650 hPa) occurred at ~0200 UTC 25 November (Fig. 12). Similar to the first storm, middle- and upper-tropospheric upward vertical motion strengthened follow-

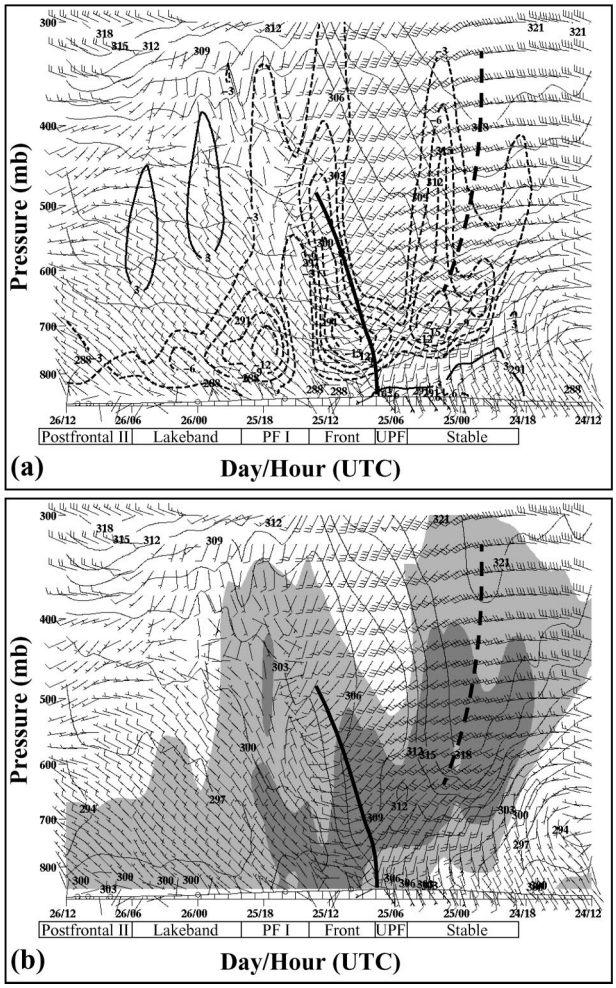

FIG. 12. Same as in Fig. 4 except for second storm (1200 UTC 24 Nov–1200 UTC 26 Nov).

ing passage of this feature, resulting in a deep layer of ascent (Fig. 12a). Widespread, generally stratiform precipitation fell until around 0500 UTC 25 November when large-scale destabilization and ascent led to the development of embedded convective cells. These embedded convective cells were evident south of CLN at 0700 UTC (Fig. 13b). Maximum reflectivities approached only 30–35 dB*Z*, suggesting that the convection was not deep or intense. Nevertheless, the development of the embedded convection resulted in an increased precipitation rate compared to the stable stage (Fig. 14, Table 2).

Also evident in Fig. 13b is precipitation along and behind a low-level cold front that was located halfway between KMTX and SLC at 0700 UTC. At this time, the 500-hPa trough axis was located over the western United States with an embedded absolute vorticity maximum just west of Las Vegas, Nevada (Fig. 16a). The primary surface low center was located along the Oregon–Idaho border, while a secondary low was found along the cold front over the Great Salt Lake basin (Fig. 16c). The cold front extended equatorward and westward to the southern Sierra Nevada and was located well behind the 700-hPa warm tongue and the remnants of the comma-shaped cirrostratus deck (Figs. 16c,d). Future work will examine the processes responsible for the development of the cold front, which appeared to form within the northern portion of the former Sierra Nevada lee trough as it moved across central and eastern Nevada. Extensive cloud cover, which developed within the dryslot, was found along and rearward of the cold front (Fig. 16d).

The surface-based cold front passed SLC and CLN at ~0800 UTC 25 November. This marked the onset of the frontal stage, which extended from 0800 to 1400 UTC and featured the passage of a convective line and a broad region of trailing stratiform precipitation (Fig. 13b) that resembled narrow and wide cold-frontal rainbands (e.g., Fig. 11.31 of Houze 1993). Observed SWEs at SLC and CLN during this frontal stage were 0.44 and 0.55 in. (1.12 and 1.40 cm), respectively (Table 2), suggesting that orographic precipitation enhancement was limited and frontal processes dominated precipitation dynamics during this period. The SLC sounding taken near the end of the frontal stage (1200 UTC 25 November), showed absolutely stable, nearly saturated conditions below 500 hPa (Fig. 15c).

Shortly after passage of the frontal precipitation zone, postfrontal destabilization resulted in a shallow layer of low-level potential instability (Fig. 12b) and the development of lake and orographically induced snowshowers (e.g., Fig. 13c). This period, denoted as postfrontal stage I, was characterized by substantial orographic precipitation enhancement, with CLN observing more than 3 times as much SWE as SLC (Table 2), although underreporting by the SLC ASOS precipitation gauge may have amplified the estimated enhancement (see section 2). Radar imagery also showed localized reflectivity maxima windward and over the crest of the Stansbury and Oquirrh Mountains (see Fig. 1 for locations), with rainshadowing to their lee (Fig. 13c). At around 2000 UTC 25 November, an intense midlake snowband developed and dominated the precipitation pattern over the next several hours (e.g., Fig. 13d). The highest precipitation rates during this storm were observed from 2200 UTC 25 November to 0000 UTC 26 November when Alta was located directly beneath the snowband and CLN observed ~0.3 in. (0.76 cm) SWE per hour (Fig. 14). Although manual snow observations were not available specifically for this period, the mean snow density collected at the base of Alta for the 12 h encompassing this period was 6%. Applying this ratio to the SWE would yield a snowfall rate of about 5 in. (12.5 cm) per hour, although it is possible that riming within the convective band increased snowfall density during this period.

Figure 17 illustrates the synoptic and mesoscale conditions at 0000 UTC 26 November when the midlake snowband was well developed. At this time, the 500-

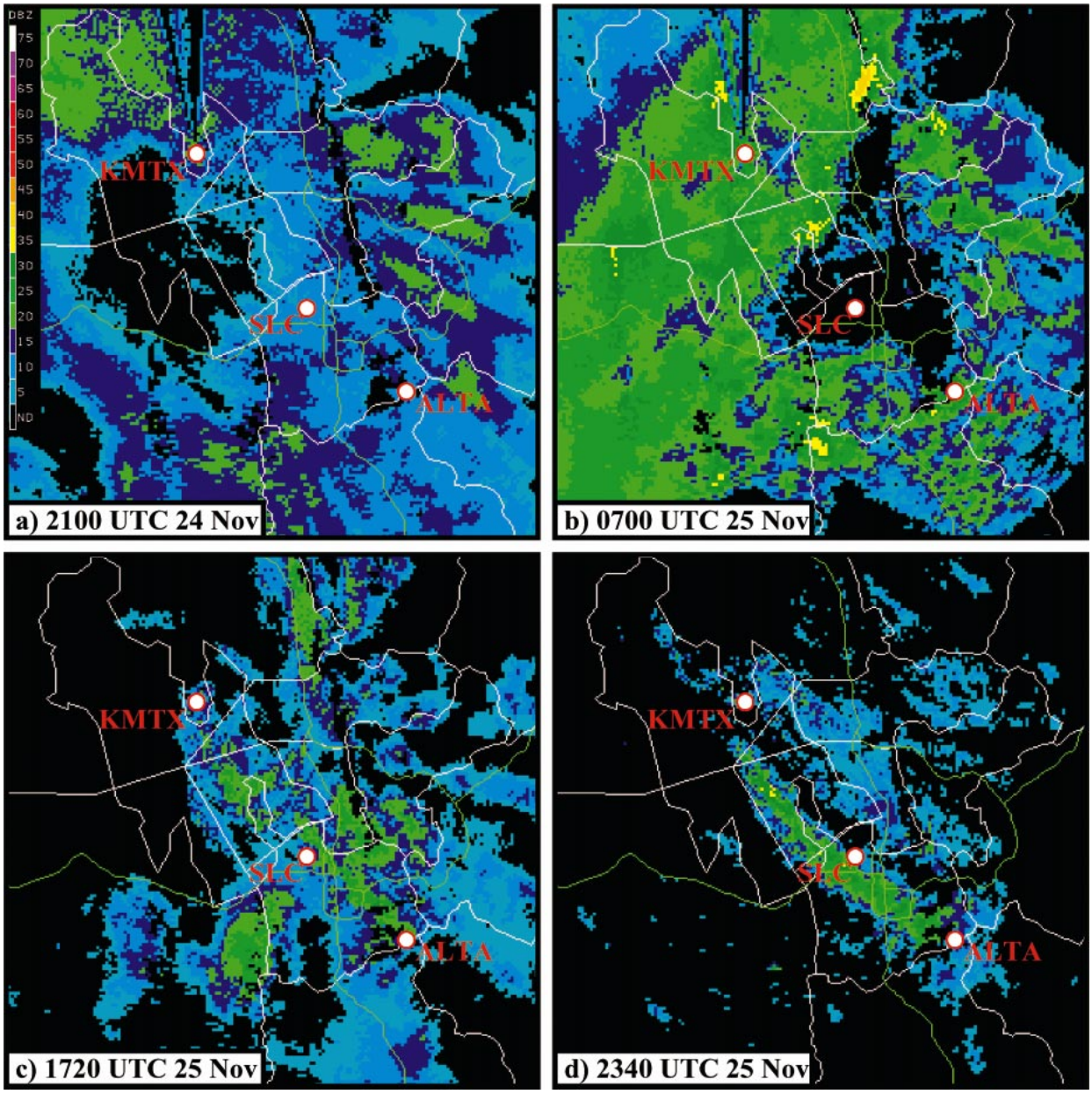

FIG. 13. KMTX lowest-elevation angle (0.5°) base reflectivity analyses at (a) 2100 UTC 24 Nov, (b) 0700 UTC 25 Nov, (c) 1720 UTC 25 Nov, and (d) 2340 UTC 25 Nov 2001.

hPa trough (Fig. 17a) and surface cyclone (not shown) were located over Colorado and SLC was under the influence of postfrontal northwesterly flow at 700 hPa (Fig. 17b). The SLC upper-air sounding showed northwesterly flow from just above the surface to near 450 hPa with near-saturated, conditionally unstable or moist-neutral lapse rates throughout this layer (Fig. 15d). Near the lakeband axis, strong westerly flow over the western portion of the Great Salt Lake appeared to converge with light flow over the eastern Great Salt Lake and adjoining Wasatch Front (Fig. 17c). Estimates of lake-wide divergence, calculated from Mesowest observations using the least squares method of Davies-Jones (1993), ranged from -1.1 to -2.1×10^{-4} s^{-1} during the lakeband period, confirming that the surface flow was convergent. Temperatures at Mesowest sites over the Great Salt Lake were 1°–4°C warmer than those found at similar elevation land-based locations around the lake. Thus, although Great Salt Lake–effect snowbands are relatively rare in the late afternoon (Steenburgh et al. 2000), sensible heat fluxes over the Great Salt Lake were able to produce offshore flow and lake-wide convergence at a time of day when onshore flow and overlake divergence are expected climatologically.

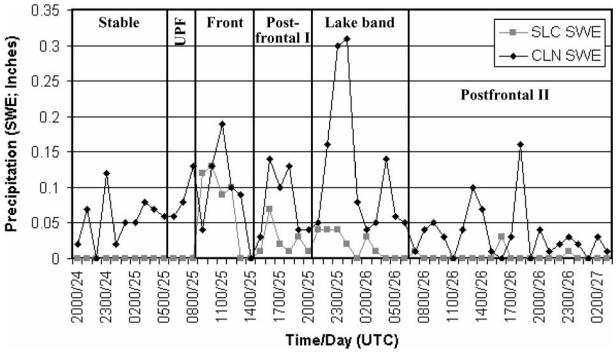

FIG. 14. Same as in Fig. 6 except for the second storm.

Precipitation at SLC and CLN was produced almost exclusively by the midlake snowband and concomitant orographic precipitation enhancement through about 0600 UTC 26 November, when the midlake band dissipated. This marked the beginning of postfrontal stage II, which featured periods of orographic and lake-effect snowshowers until 0300 UTC 27 November. As observed during the final stage of the preceding storm, precipitation was confined almost exclusively to the mountains, with CLN receiving 0.70 in. (1.78 cm) SWE compared to only 0.05 in. (0.13 cm) at SLC.

Similar to the preceding storm, approximately two-thirds (64%) of the storm total SWE observed at CLN during this second storm was produced by postfrontal orographic and lake-effect snowshowers. Thirty-three percent of the storm total was produced during a period when a midlake snowband extended from the Great Salt Lake over CLN. Combined, the two storms produced 63% of the CLN SWE in the postfrontal environment, with 26% produced exclusively by midlake snowbands and their interaction with the Wasatch Mountains. Lake-effect processes were also partially responsible for precipitation during postfrontal periods when midlake bands were not dominant, suggesting that they were responsible for at least one-third of the total SWE.

4. Discussion

a. Storm evolution

As noted in the introduction, several authors have described the evolution of orographic snowstorms using stages based on stability and/or the passage of transient synoptic features such as surface-based or upper-level fronts and baroclinic zones (e.g., Hobbs 1975; Marwitz 1980; Marwitz and Cooper 1980; Long et al. 1990). In contrast to the conceptual models of Hobbs (1975), Marwitz (1980), and Marwitz and Cooper (1980), which describe a storm evolution featuring only three major storm stages (stable, neutral, and unstable), the storms examined in the present paper featured a more complex series of storm stages. Specifically, each storm featured the passage of an occluded-like warm tongue and leading edge of low-θ_e air aloft followed several hours later by a surface-based cold frontal passage. The intrusion of low-θ_e air aloft resulted in a transition from stable to convective precipitation, while the surface cold front was accompanied by a convective line and trailing region of stable, stratiform precipitation, which, in the second storm, resembled narrow and wide cold frontal rainbands. Destabilization of the postfrontal environment ultimately resulted in another unstable period that included the development of lake and orographically induced convective snowshowers. Identification of this complex series of storm stages was aided by high-resolution operational observing and analysis systems, such as the KMTX WSR-88D and hourly RUC2 analyses.

This storm evolution is more consistent with that described by Long et al. (1990) and Sassen et al. (1990) for a winter storm in the Tushar Mountains, which are located in south-central Utah. As illustrated by Fig. 4 of Long et al. (1990), the Tushar Mountain winter storm featured the passage of an upper-level ''cold surge/humidity front'' that was located ahead of a surface-based cold front. Passage of the upper-level cold surge/hu-

TABLE 2. Precipitation characteristics of the major stages of the second storm.

Stage and time period	CLN SWE (in.)	CLN mean SWE rate (in. h^{-1})	Contribution to CLN storm total SWE (%)	SLC SWE (in.)	SLC mean SWE rate (in. h^{-1})	Contribution to SLC storm total SWE (%)	Orographic enhancement (CLN/SLC) (%)
Stable, 1900 UTC 24 Nov–0500 UTC 25 Nov	0.54	0.054	14.3	0	0	0	—
Unstable prefrontal, 0500–0800 UTC 25 Nov	0.27	0.090	7.1	0	0	0	—
Frontal passage, 0800–1400 UTC 25 Nov	0.55	0.092	14.6	0.44	0.073	53.7	125
Postfrontal I, 1400–2000 UTC 25 Nov	0.48	0.080	12.7	0.15	0.025	18.3	313
Midlake band, 2000 UTC 25 Nov–0600 UTC 26 Nov	1.24	0.124	32.8	0.18	0.018	21.9	689
Postfrontal II, 0600 UTC 26 Nov–0300 UTC 27 Nov	0.70	0.033	18.5	0.05	0.002	6.1	1400
Total, 1900 UTC 24 Nov–0300 UTC 27 Nov	3.78	0.071	100	0.82	0.015	100	461

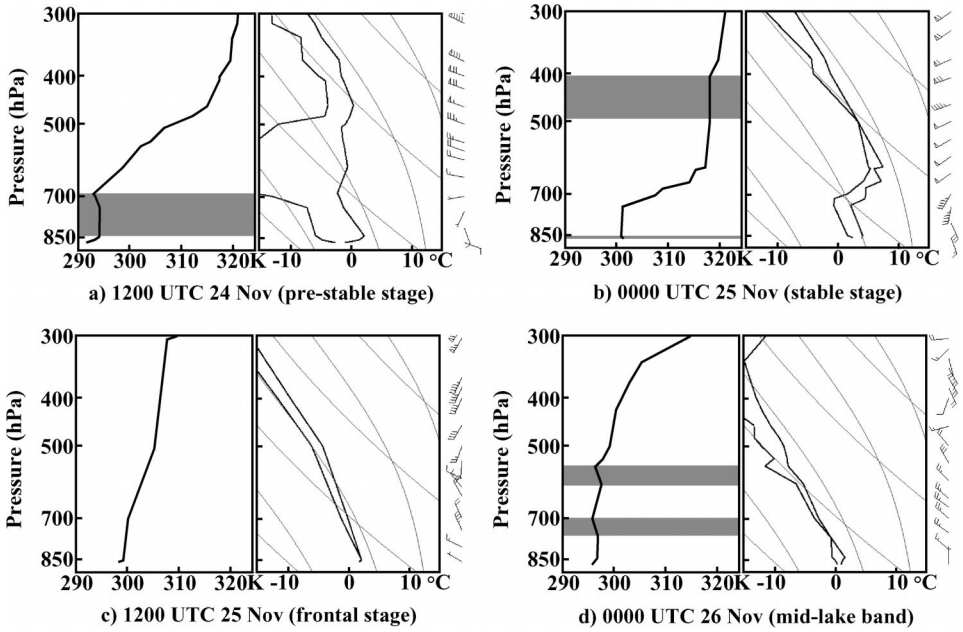

FIG. 15. Same as in Fig. 7 except for (a) 1200 UTC 24 Nov, (b) 0000 UTC 25 Nov, (c) 1200 UTC 25 Nov, and (d) 0000 UTC 26 Nov 2001.

midity front resulted in a transition from stable to unstable cloud and precipitation processes. Passage of the cold front resulted in a period where frontal lifting dominated precipitation production. This evolution is similar to that described for the two storms responsible for the 100-in. storm cycle, with the warm tongue and leading edge of low-θ_e aloft analogous to the upper-level cold surge/humidity front of Long et al. (1990).

One difference between the events, however, is the prolonged periods of heavy, postfrontal, orographic and lake-effect snowshowers that were observed during the 100-in. storm cycle. This was the result of two factors. First, the postfrontal environment in the Long et al. (1990) event featured a low-level intrusion of cold, dry air that resulted in the development of convectively stable conditions. In contrast, the storms responsible for the 100-in. storm cycle featured potentially unstable postfrontal environments. This illustrates the importance of evaluating the postfrontal convective environment on a case-by-case basis. Second, postfrontal precipitation during the 100-in. storm cycle was greatly augmented by lake-effect precipitation processes, which are unique to the Wasatch Mountains due to their close proximity to the Great Salt Lake.

An important unanswered question concerns the origin of the prefrontal intrusion of low-θ_e air aloft. A number of papers have described similar features, including the split cold front of Browning and Monk (1982) and cold front aloft of Hobbs et al. (1990, 1996). Unlike the split front model of Browning and Monk (1982), however, the storms that produced the 100-in. storm cycle featured a well-defined zone of precipitation along and immediately behind the cold front. The storms also contrast with the Hobbs et al. (1990, 1996) cold front aloft model since convection was not organized along the leading edge of low-θ_e air aloft.

There are several possible reasons why low-θ_e air aloft might be found ahead of surface-based cold fronts over the Intermountain West. First, the region lies downstream of the Pacific storm track (e.g., Zishka and Smith 1980) and many fronts traversing the region are occluded as they make landfall onto the Pacific coast. As a result, the leading edge of low-θ_e air aloft may simply be a remnant of the elevated cold front of the occlusion. This does not, however, explain the existence of a well-defined surface-based cold front and associated precipitation bands. Another possibility is that the leading edge of low-θ_e air aloft develops from the confluence of relatively dry, descended trajectories originating behind the upper-level trough with relatively moist, ascended trajectories originating well ahead of the approaching storm. This process is similar to that which produced an upper-level humidity front in an eastern U.S. cyclogenesis event examined by Mass and Schultz (1993), although the 100-in. storm cycle differed in two ways. First, the leading edge of low-θ_e air aloft represented a transition in moisture *and* temperature (Figs. 4, 12), whereas the Mass and Schultz (1993) event featured a transition between moist and dry air of roughly equal temperature. Second, the surface-based cold front in the Mass and Schultz (1993) event was not accompanied by clouds and precipitation.

Separation between the leading edge of low-θ_e air aloft and the surface-based cold front may be created or enhanced by topographic effects. For example, the Sierra Nevada and Great Basin ranges may retard the

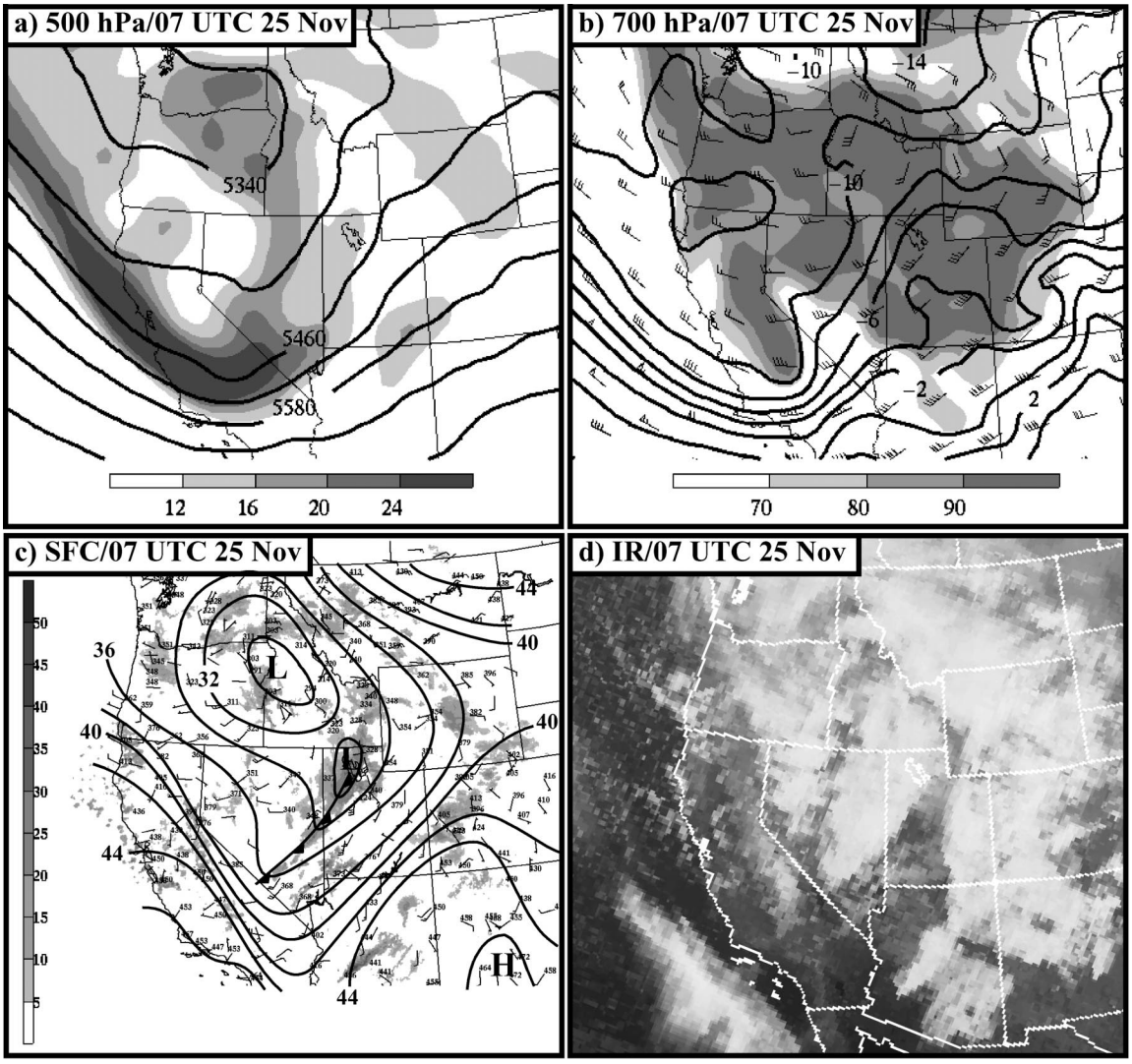

FIG. 16. Same as in Fig. 3 except for 0700 UTC 25 Nov 2001 and thermal ridge no longer analyzed in (b).

progression of the surface-based cold front, while low-θ_e air aloft moves freely downstream. Alternatively, in a manner similar to that envisioned by Smith (1982), a vertically continuous frontal zone may steepen, become tipped forward, and decouple as it traverses the Sierra Nevada and Great Basin ranges. In such a scenario, the low-level portion of the cold front might remain blocked on the western slopes of the Sierra Nevada, with a new cold front forming over Nevada behind the leading edge of low-θ_e air aloft. Future work should examine how large-scale and topographic features create structures similar to those observed during the 100-in. storm cycle, including the contributions of the above mechanisms.

b. A summary schematic

Based on the analysis of the two storms responsible for the 100-in. storm cycle, the work of Long et al. (1990), and investigations of other northern Utah snowstorms (e.g., Shafer 2002), Fig. 18 presents a schematic diagram summarizing the evolution of orographic precipitation processes during events that feature an intrusion of low-θ_e air aloft ahead of a surface-based cold front. Prior to the intrusion of low-θ_e air, stable precipitation processes dominate and contrasts between lowland and mountain precipitation are produced by shallow upslope precipitation enhancement at mid- and upper-mountain levels and subcloud evaporation over the lowlands. As low-θ_e air moves in aloft, destabilization results in convection (provided large-scale or orographic ascent is present to release the instability). The intensity and depth of the convection, as well as the lowland–mountain precipitation contrast, varies significantly from case to case depending on the ambient instability, moisture, and convective initiation mechanisms.

Passage of the low-level cold front results in a period

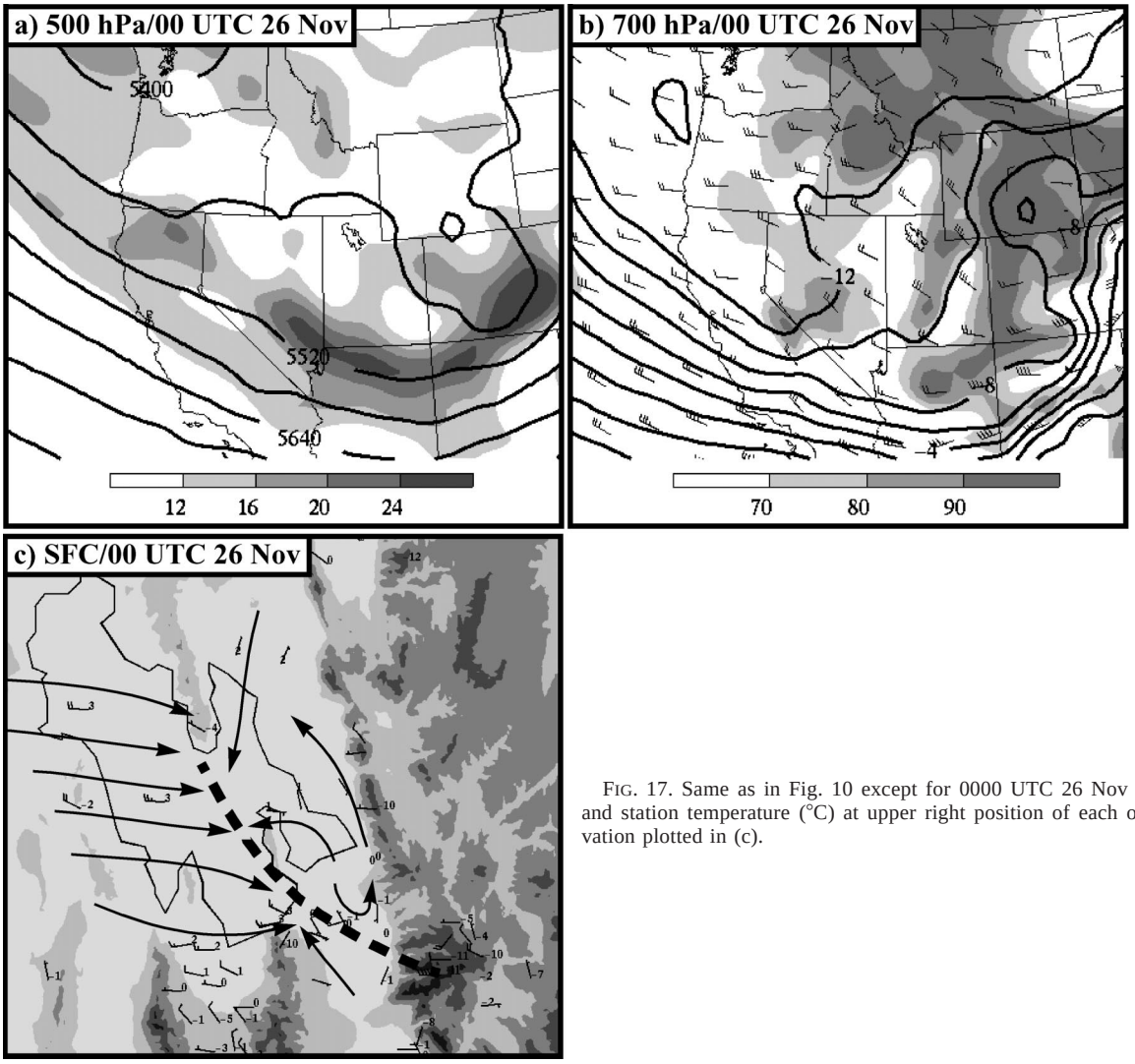

FIG. 17. Same as in Fig. 10 except for 0000 UTC 26 Nov 2001 and station temperature (°C) at upper right position of each observation plotted in (c).

where frontal dynamics dominate precipitation generation over lowland and mountain locations. Then, large-scale destabilization results in orographic snowshowers due to the release of potential instability, although precipitation rate and duration are dependent upon the convective characteristics of the postfrontal environment and size and orientation of the local topography. Precipitation during this stage is confined primarily to over the mountain barrier unless other processes, such as the Great Salt Lake effect or terrain-induced convergence, act to generate precipitation.

The schematic summarizes one type of winter storm evolution that occurs over the Wasatch Mountains and other ranges of the Intermountain West. Because no single storm type dominates orographic snowfall production in this region, additional work is needed to determine its commonality and to identify how other large-scale flow configurations influence the evolution of Intermountain West winter storms.

c. Implications for weather and climate prediction

A strong correlation between precipitation and altitude dominates the climatology of the Intermountain West (Daly et al. 1994). For example, over northern Utah, climatology features a nearly fourfold difference in precipitation between the Salt Lake valley (e.g., SLC) and the upper elevations of the Wasatch Mountains (e.g., CLN; Dunn 1983). Meteorologists frequently utilize this climatological altitude–precipitation relationship to predict the mesoscale distribution of precipitation, with some modifications based on flow direction and static stability (L. Dunn 2002, personal communication).

The results presented in the present paper, however, show considerable variability in the lowland to mountain precipitation contrast from storm to storm and stage to stage (Tables 1 and 2). During the first storm, CLN received 245% more precipitation than SLC, with the contrast varying from as little as 180% during the un-

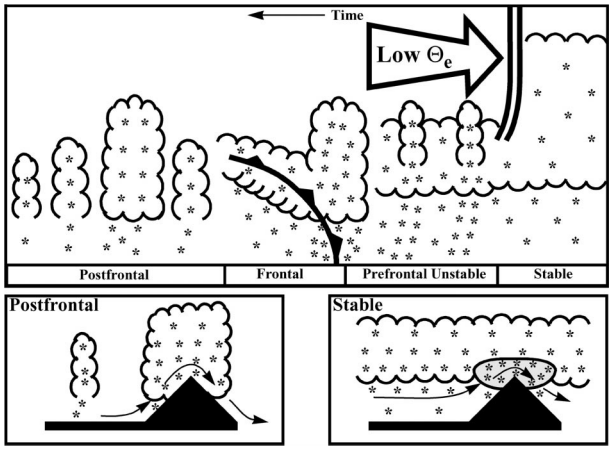

FIG. 18. Schematic diagram describing the evolution of Intermountain West storms featuring an intrusion of low-θ_e air aloft ahead of a surface-based cold front. Lower portion of diagram depicts orographic effects during stable and postfrontal unstable stages.

stable prefrontal stage to as much as 500% in postfrontal stage II when convection was located almost exclusively over the mountains. In contrast, during the second storm, CLN received 461% more precipitation than SLC (this ratio was enhanced slightly due to underreporting by the SLC ASOS gauge), with the contrast varying from as little as 125% during the frontal stage, to undefined during the stable and unstable prefrontal periods when CLN received 0.81 in. (2.1 cm) SWE, while SLC recorded no measurable precipitation.

These results illustrate the difficulties of applying the climatological altitude–precipitation relationship for short-range forecasting. Considerable departures from this relationship must be expected from stage to stage and storm to storm. These departures will be particularly problematic for the production of gridded quantitative precipitation forecasts, which the National Weather Service plans to produce as an operational product beginning in October 2003.

Another concern lies in the area of seasonal and annual hydrometeorological prediction. As noted in the introduction, this one storm cycle, which covered a 5-day period, produced 15% of the SWE that fell in Salt Lake City watersheds during winter 2001/02. In addition, a significant fraction of the storm cycle precipitation was produced by lake-effect precipitation processes. This illustrates the importance of accurately accounting for the Great Salt Lake in coupled hydrometeorological prediction models applied for seasonal or annual water resource management over northern Utah.

5. Summary and conclusions

From 22 to 27 November 2001, two major winter storms produced 108 in. (274 cm) of snow at Alta Ski Area, with 100 in. (254 cm) falling during a 100-h period. Each storm system featured an intrusion of low-θ_e air aloft, followed several hours later by the passage of a surface-based cold front. Precipitation became increasingly convective following passage of the leading edge of low-θ_e air aloft, while cold frontal passage was accompanied by a convective line and stratiform precipitation region, which during the second event resembled narrow and wide cold frontal rainbands. In both cases, postfrontal destabilization led to a prolonged period of heavy orographic and lake-effect snowshowers, including times with intense midlake snowbands.

Contrasts between mountain and lowland precipitation varied widely from storm to storm and stage to stage. In general, the magnitude of orographic precipitation enhancement was largest during the stable (i.e., prior to the intrusion of low-θ_e air aloft) and postfrontal stages. Hydrometeor evaporation in the subsaturated air mass resident over the Salt Lake valley, combined with precipitation enhancement within a shallow layer of upslope flow at mid- and upper-mountain levels, appeared to produce the contrast during the stable stage. Contrasts during postfrontal periods arose from orographic precipitation enhancement within lake-effect snowbands and the tendency of convective snowshowers to be confined primarily to over the mountains during periods when lake-effect snowbands were not present. Almost two-thirds of the total storm cycle SWE at Alta Ski Area (63%) was produced by postfrontal precipitation. Orographically enhanced lake-effect snowbands appeared to be responsible for half of this postfrontal precipitation, or roughly one-third of the storm cycle total.

A schematic diagram was developed to summarize the evolution of synoptic features and precipitation processes in this and other storms featuring prefrontal intrusions of low-θ_e air aloft. Events of this type may be relatively common over the Intermountain West since other studies in this region have documented similar evolutions (e.g., Long et al. 1990; Shafer 2002). Future work should examine the factors responsible for the development of the prefrontal intrusions of low-θ_e air aloft, including the contributions of synoptic and orographic processes.

Acknowledgments. Ethan Greene of the Utah Avalanche Center and Larry Dunn of the National Weather Service stimulated and encouraged this study. Special thanks to the Mesowest cooperative networks, including John Horel, Mike Splitt, Judy Pechmann, and Bryan White; Dan ''Howie'' Howlett of the Alta Snow Safety Staff; and Linda Cheng of the National Weather Service SLC Forecast Office, for providing surface observations and precipitation data. Mike Splitt also provided estimates of lakewide divergence. Jason Shafer, Dave Schultz, and three anonymous reviewers provided insightful discussion and comments that enhanced the manuscript. This work was sponsored by National Science Foundation Grant ATM-0085318 and a series of grants provided by the National Weather Service C-

STAR program to the NOAA/Cooperative Institute for Regional Prediction at the University of Utah.

REFERENCES

Benjamin, S. G., J. M. Brown, K. J. Brundage, B. E. Schwartz, T. G. Smirnova, T. L. Smith, and L. L. Marone, 1998: RUC-2—The Rapid Update Cycle version 2. NWS Tech. Procedure Bull. 448, NOAA/NWS, 18 pp. [Available from Office of Meteorology, National Weather Service, 1325 East–West Highway, Silver Spring, MD 20910.]

Browning, K. A., and G. A. Monk, 1982: A simple model for the synoptic analysis of cold fronts. *Quart. J. Roy. Meteor. Soc.*, **108,** 435–452.

Cooper, W. A., and J. D. Marwitz, 1980: Winter storms over the San Juan Mountains. Part III: Seeding potential. *J. Appl. Meteor.*, **19,** 942–949.

Cox, J. A. W., 2002: Kinematic structure of a Wasatch Mountain snowstorm. M.S. thesis. Dept. of Meteorology, University of Utah, 60 pp. [Available from Dept. of Meteorology, University of Utah, 135 South 1460 East, Rm. 819, Salt Lake City, UT 84112-0110.]

Crum, T. D., and R. L. Alberty, 1993: The WSR-88D and the WSR-88D operational support facility. *Bull. Amer. Meteor. Soc.*, **74,** 1669–1687.

Daly, C., R. P. Neilson, and D. L. Phillips, 1994: A statistical–topographic model for mapping climatological precipitation over mountainous terrain. *J. Appl. Meteor.*, **33,** 140–158.

Davies-Jones, R., 1993: Useful formulas for computing divergence, vorticity, and their errors from three or more stations. *Mon. Wea. Rev.*, **121,** 713–725.

Dunn, L. B., 1983: Quantitative and spacial [sic] distribution of winter precipitation along Utah's Wasatch Front. NOAA Tech. Memo. NWS WR-181, 72 pp. [Available from NOAA/NWS Western Region Headquarters, 125 S. State St., Rm. 1311, Salt Lake City, UT 84138-1102.]

——, and S. V. Vasiloff, 2001: Tornadogenesis and operational considerations of the 11 August 1999 Salt Lake City tornado as seen from two different Doppler radars. *Wea. Forecasting*, **16,** 377–398.

Hobbs, P. V., 1975: The nature of winter clouds and precipitation in the Cascade Mountains and their modification by artificial seeding. Part I: Natural conditions. *J. Appl. Meteor.*, **14,** 783–804.

——, J. D. Locatelli, and J. E. Martin, 1990: Cold fronts aloft and the forecasting of precipitation and severe weather east of the Rocky Mountains. *Wea. Forecasting*, **5,** 613–626.

——, ——, and ——, 1996: A new conceptual model for cyclones generated in the lee of the Rocky Mountains. *Bull. Amer. Meteor. Soc.*, **77,** 1169–1178.

Holton, J. R., 1992: *An Introduction to Dynamic Meteorology.* 3d ed. Academic Press, 511 pp.

Horel, J., and Coauthors, 2002: Mesowest: Cooperative mesonets in the western United States. *Bull. Amer. Meteor. Soc.*, **83,** 211–226.

Houze, R. A., Jr., 1993: *Cloud Dynamics.* Academic Press, 573 pp.

Long, A. B., B. A. Campistron, and A. W. Huggins, 1990: Investigations of a winter mountain storm in Utah. Part I: Synoptic analyses, mesoscale kinematics, and water release rates. *J. Atmos. Sci.*, **47,** 1302–1322.

Marwitz, J. D., 1980: Winter storms over the San Juan Mountains. Part I: Dynamical processes. *J. Appl. Meteor.*, **19,** 913–926.

——, 1986: A comparison of winter orographic storms over the San Juan Mountains and the Sierra Nevada. *Precipitation Enhancement—A Scientific Challenge, Meteor. Monogr.*, No. 43, Amer. Meteor. Soc., 109–113.

Mass, C. F., and D. M. Schultz, 1993: The structure and evolution of a simulated midlatitude cyclone over land. *Mon. Wea. Rev.*, **121,** 889–917.

Onton, D. J., and W. J. Steenburgh, 2001: Diagnostic and sensitivity studies of the 7 December 1998 Great Salt Lake–effect snowstorm. *Mon. Wea. Rev.*, **129,** 1318–1338.

Pope, D., and C. Brough, 1996: *Utah's Weather and Climate.* Publishers Press, 245 pp. [Available from Publishers Press, 1900 West 2300 South, Salt Lake City, UT 84119.]

Sassen, K., A. W. Huggins, A. B. Long, J. B. Snider, and R. J. Meitín, 1990: Investigations of a winter mountain storm in Utah. Part II: Mesoscale structure, supercooled liquid water development, and precipitation processes. *J. Atmos. Sci.*, **47,** 1323–1350.

Shafer, J. C., 2002: Synoptic and mesoscale structure of a Wasatch Mountain winter storm. M.S. thesis, Dept. of Meteorology, University of Utah, 65 pp. [Available from Dept. of Meteorology, University of Utah, 135 South 1460 East, Rm. 819, Salt Lake City, UT 84112-0110.]

Smith, R. B., 1982: A differential advection model of orographic rain. *Mon. Wea. Rev.*, **110,** 306–309.

Steenburgh, W. J., and T. R. Blazek, 2001: Topographic distortion of a cold front over the Snake River plain and central Idaho mountains. *Wea. Forecasting*, **16,** 301–314.

——, and D. J. Onton, 2001: Multiscale analysis of the 7 December 1998 Great Salt Lake–effect snowstorm. *Mon. Wea. Rev.*, **129,** 1296–1317.

——, S. F. Halvorson, and D. J. Onton, 2000: Climatology of lake-effect snowstorms of the Great Salt Lake. *Mon. Wea. Rev.*, **128,** 709–727.

Stoelinga, M. T., J. D. Locatelli, and P. V. Hobbs, 2000: Structure and evolution of winter cyclones in the central United States and their effects on the distribution of precipitation. Part VI: A mesoscale modeling study of the initiation of convective rainbands. *Mon. Wea. Rev.*, **128,** 3481–3500.

Wallace, J. M., and P. V. Hobbs, 1977: *Atmospheric Science: An Introductory Survey.* Academic Press, 467 pp.

Zishka, K. M., and P. J. Smith, 1980: The climatology of cyclones and anticyclones over North America and surrounding ocean environs for January and July, 1950–77. *Mon. Wea. Rev.*, **108,** 387–401.